ACS APPLIED POLYMER MATERIALS

Article

Cite This: ACS Appl. Polym. Mater. 2019, 1, 982−989

pubs.acs.org/acsapm

Architecture Can Significantly Alter the Energy Release Rate from Nanocomposite Energetics

Haiyang Wang,[†,‡] Dylan Jacob Kline,[†] Miles Rehwoldt,[†] Tao Wu,[†] Wanjun Zhao,[†] Xizheng Wang,[†] and Michael R. Zachariah[†,‡,*]

[†]Department of Chemical and Biomolecular Engineering and Department of Chemistry and Biochemistry, University of Maryland, College Park, Maryland 20742, United States

[‡]Department of Chemical and Environmental Engineering, University of California, Riverside, California 92521, United States

Supporting Information

ABSTRACT: With the advent of additive manufacturing methods combined with the increased interest in using nanoparticle components to formulate energetics materials, structure−function relationships and manufacturing methods have become intertwined. In this article, we explore three different approaches to formulate composites and evaluate the combustion properties. Here polyvinylidene fluoride (PVDF) was used to assemble both aluminum nanoparticles (Al NPs) and ammonium perchlorate (AP). Three different fabrication techniques, 3D-print, electrospray (E-spray), and electrospin (E-spin), were employed in this work. Composites of Al/PVDF and composites with a high oxidizer content, employing AP, were studied. The relationship between architecture and the burning rate of both Al/PVDF and Al/AP/PVDF was investigated by studying the thermal decomposition at high and low heating rates, and flame temperatures via the color camera pyrometry on microscale ignition/combustion events. By studying the release of HF, ignition temperatures, and the flame front, we propose a mechanism for the combustion of the multicomponent energetic films. Flame temperature, completeness of reaction, and a significant difference in ignition temperature appear to favor the E-spray material. However, the large difference in propagation velocity between E-spray and E-spun, given the minor difference in density, clearly points to the importance of microarchitecture on reaction properties. The relative energy release rate of E-spun Al/PVDF compared to the E-sprayed and 3-D printed case is an enhancement of ∼6× and 18×, respectively, and the energy release rate of E-spun Al/AP/PVDF is ∼19× higher than that of E-sprayed and 3D-printed samples. This implies that the lowest density spun material offers the highest mass energy release rate by far.

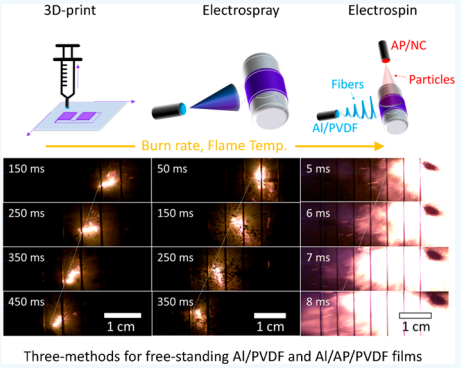

Three-methods for free-standing Al/PVDF and Al/AP/PVDF films

KEYWORDS: *PVDF, fibers, 3D printing, electrospray, electrospin*

INTRODUCTION

The architecture of the energetic composites is known to play an important role in combustion behavior. Li et al.[1] showed that the formation of laminated thermite layers polyvinylidene fluoride (PVDF) spacer layers burned 25% faster than the equivalent single layer film. More recently, we found that the addition of 5 wt % meso-silica particles highly promotes the decomposition of PVDF and induces a multilayered structure, thus increasing the burning rate to ∼30 cm/s.[2] Yan et al. produced Al/CuO/NC fibers which can burn at velocities of ∼100 cm/s, while the same composition film cannot propagate.[3] Li et al. also imbedded PVDF fibers into Al/CuO/PVDF films and observed a 1.8× higher burning rate.[4] More recently, we produced laminated Al/PVDF/iodine films by a dual-nozzle electrospraying technique, which propagated at ∼5 cm/s with an iodine content as high as 67 wt %. In contrast, the same overall composition in a single-layered Al/PVDF/I_2 could not propagate with an I_2 content >35 wt %.[5] Sullivan et al.[6] found that the orientation and spacing of the reactive Al/CuO with different architectures significantly impact the propagation velocity, probably due to dynamics of the multiphase expansion process.

With the advent of additive manufacturing methods combined with the increased interest in using nanoparticle components to formulate energetics materials, structure−function relationships[1−6] and manufacturing methods[7−16] have become intertwined. In this article, we explore three different approaches to formulate composites and evaluate the combustion properties. In this study, we employ PVDF as a versatile candidate polymer to prepare propellants as both a binder and an oxidizer with superior mechanical properties. The strong Al−F bond also implies that the heat of reaction should be very favorable compared to the formation of alumina.[7−9] Although Al/Teflon has been widely investigated

Received: January 8, 2019
Accepted: March 5, 2019
Published: March 5, 2019

DOI: 10.1021/acsapm.9b00016
ACS Appl. Polym. Mater. 2019, 1, 982−989

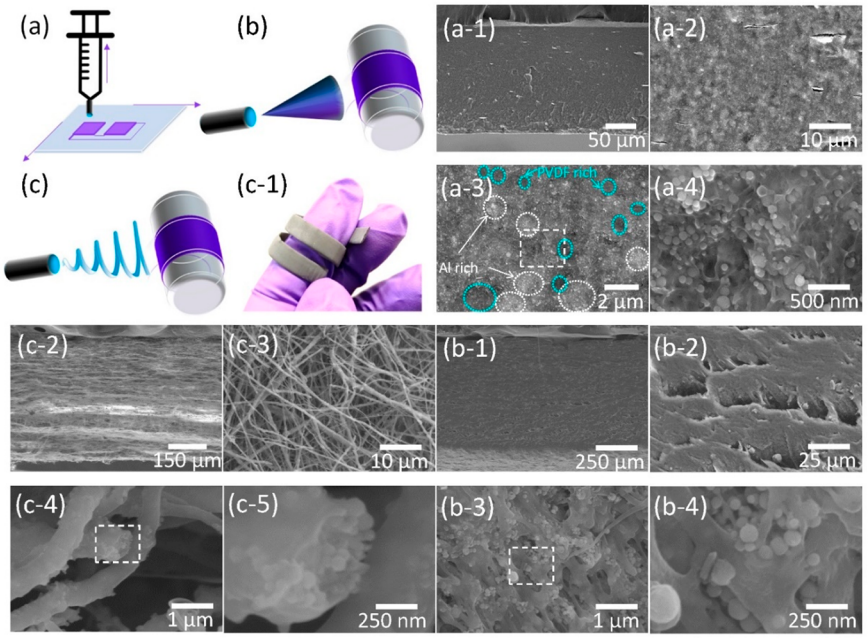

Figure 1. Schematic showing of 3D-printing (a), E-spraying (b), and E-spinning deposition (c) of Al/PVDF films. The photo of the E-spun Al/PVDF fiber film (c-1, ~ 15 cm × 0.5 cm). The cross-sectional SEM images from low to high magnification of 3D-printed (a-1 to a-4), E-sprayed (b-1 to b-4), and E-spun (c-2 to c-5). Note, that the thicknesses for 3D-printed, E-sprayed, and E-spun films are ~200, ~ 600, and ~500 μm.

in recent years,[17] the solubility and low melting point of PVDF make it an attractive 3D-printable energetic binder despite its lower fluorine concentration. Huang et al.[7] dissolved PVDF in dimethyl furan (DMF) and obtained a homogeneous suspension to prepare a free-standing thin film via an electrospray (E-spray) deposition technique. Al/PVDF films have superior mechanical properties, even when the Al content is as high as 50 wt %.[7] In addition to the work discussed above, the PVDF low melting point enabled McCollum et al.[8] extrusion Al/PVDF into thin filaments to prepare Al/PVDF films through 3D-printing. The above studies suggest that an intercomparison of structures fabricated by different additive manufacturing methods might yield interesting and useful insights.

Here, PVDF was used to assemble both Al NPs and ammonium perchlorate (AP). Three different fabrication techniques, 3D-print, electrospray (E-spray), and electrospin (E-spin), were employed in this work. Composites of Al/PVDF and composites with a high oxidizer content, employing AP, were studied. The relationship between architecture and the burning rate of both Al/PVDF and Al/AP/PVDF was investigated by studying the thermal decomposition at high and low heating rates and flame temperatures via color camera pyrometry on microscale ignition/combustion events. By studying the release of HF, ignition temperatures, and the flame front, we propose a mechanism for the combustion of the multicomponent energetic films.

EXPERIMENTAL SECTION

Chemicals and Precursors. Aluminum nanoparticles (Al NPs, ~ 85 nm) were purchased from Novacentrix. The active aluminum content is ~81 wt % according to the thermogravimetry/differential scanning calorimetry (TG/DSC) results. PVDF (534 000), methanol, and acetone were purchased from Sigma-Aldrich. *N*,*N*-Dimethylformamide (DMF, 99.8%) was purchased from BDH chemicals. All chemicals were used as received. When calculating the equivalence ratio, the active Al content was taken into consideration. As an example, for an Al/PVDF precursor (with an equivalence ratio of 1.5), 450 mg of PVDF was dissolved in 4.5 mL of DMF, and following dissolution, 235 mg of Al NPs were then added into the solution and sonicated for 1 h. After being stirred for 24 h, the suspension was ready for E-spraying and 3D-printing. For the E-spinning case, 1.5 mL of the DMF was replaced with acetone. For an Al/AP/PVDF precursor (stoichiometric) used by E-spraying and 3D-printing, 165.6 mg of AP and 18.4 mg of NC were dissolved with the PVDF in the DMF solution. For the Al/AP/PVDF precursors used by E-spinning, in addition to the above Al/PVDF vial, a separate vial of AP/NC solution was made, in which 165.6 mg of AP and 18.4 mg of NC were dissolved in a mixture of 0.5 mL of acetone and 2.5 mL of methanol.[18]

E-spray, E-spin, and 3D-print of Al/PVDF and Al/AP/PVDF Free-Standing Films. The details of the E-spraying and E-spinning setup can be found in our previous studies.[19,20] For both E-sprayed and E-spun Al/PVDF films, the precursor was sprayed with a single nozzle. For the E-spun Al/AP/PVDF films, the Al/PVDF part was the same as above, and an additional nozzle was employed to spray AP/NC. The 3D-printer used was purchased from Hyrel 3D (Hyrel System 30M) and had a heating stage (~80 °C) to evaporate DMF to form a film in situ. The precursor was loaded in a 30 mL syringe with a feed rate of ~4.5 mL/h (measured feed rate) and a needle size of ~0.7 mm. The printed area was 2 cm × 2 cm, shown in Figure S1. The thickness of the film was determined by scanning electron microscopy (SEM). The mass of each film was measured with a resolution of 0.1 mg, and from the dimension, the density was calculated. At least four samples were employed to get the average density with a standard error.

SEM, EDS, XRD, and TG/DSC/MS. The microstructure of Al/PVDF and Al/AP/PVDF films was investigated by using a Hitachi SU-70 scanning electron microscope coupled to an energy dispersive spectrometer (EDS). The films were sectioned in liquid nitrogen and attached to a carbon film on an SEM stage. Films were also characterized by powder X-ray diffraction (XRD, Bruker D8 with Cu K radiation) and thermogravimetry/differential scanning calorimetry/mass spectrometry (TG/DSC/MS, TA Instruments Q600 and Discovery Mass spectrometer, with an argon flow of 100 mL/min and a heating rate of 10 °C/min).

Burning Rate Measurement and Flame Temperature Estimation. Films were cut to 3 cm × 0.5 cm (E-spray and E-spin) or 2 cm × 0.5 cm (3D-print) sections for burning rate tests and

DOI: 10.1021/acsapm.9b00016
ACS Appl. Polym. Mater. 2019, 1, 982−989

air-dried overnight. The films were ignited with a Joule-heated nichrome wire (~1 cm in length, 0.010 in. in diameter) in a quartz tube filled with argon in advance (10 L/min argon flow for 5 min). Film burning was recorded using a high-speed camera at a rate of 5000−7000 pps (Vision Research Phantom Miro M110 high-speed camera). For measuring the burning rate in water, the film was adhered on the bottom of a 5 mL beaker by using a small piece of double-side tape, such that ~2−3 mm of the film remained above the water surface for ignition. All the tests were conducted in triplicate, and the average burning rate with standard error are reported.

To estimate temperature of the burning films, color ratio pyrometry was performed using the same high-speed color camera. By taking ratios of raw channel intensities, dependency on most variables associated with intensity was eliminated, except for those regarding the channel gain, emissivity, and spectral response of the camera at individual wavelengths and channels.[21] According to a modified Graybody assumption and then a fitted Planck's Law,[22,23] the temperatures raw data (pixel values) were obtained and then calibrated (773−4773K) with a Newport Oriel 67000 Series Blackbody Infrared Light Source.[24] MATLAB was used to extract raw pixel values and calculate temperatures. Three color ratios (green/red, blue/green, and blue/red) were simultaneously used to estimate temperature by minimizing their summed error (nominally ~110 K) from theoretical ratios. For the figures that show a temperature of a single sample as a function of time, only unsaturated pixels above the black level and within the error threshold were used to report the mean temperature of the frame for a contiguous area of at least 10 acceptable pixels.

T-Jump Ignition and Time-of-Flight Mass Spectrometry. The details of the T-jump time-of-flight mass spectrometry (T-Jump MS) method to determine ignition temperature and the temporal evolution of species can be found in ref 25. Typically, when conducting the 3D-printing, E-spraying, and E-spinning, a ~ 10 mm long platinum filament (~76 μm in diameter) was coated with the Al/PVDF (~15−20 μm thickness). The coating method for E-spinning was the same as the E-spraying case, which can be found in ref 20. For 3D-printing, the filament was placed on the print plain and was coated with a thickness of ~15−20 μm. The filament was resistively heated to ~1400 K (heating rate of ~4×10^5 K·s^{-1}, in 1 atm of argon). The ignition and subsequent combustion of the composite was monitored using a high-speed camera (14.9 μs exposure with 256 × 256 pixels, Phantom V12.1, 76000 pps). The temporal wire resistance (correlated via the Callendar-Van Dusen equation) during the heating process was recorded, and the ignition temperature was calculated by coupling the observed ignition timestamp from the high-speed video with the wire temperature. A high speed, time-of-flight mass spectrometer was also coupled with to the ignition filament, which was used for detecting the species released during fast heating.

RESULTS AND DISCUSSION

Architecture of Al/PVDF Films: 3D-Printing, E-Spraying, and E-Spinning. Al/PVDF films with equivalence ratios of 0.5, 1.0, and 1.5 (wt % of Al is ~15, ~25, and ~35%, respectively) were prepared by 3D-printing (Figure 1a), E-spraying (Figure 1b), and E-spinning (Figure 1c). Of the films prepared, 3D-prining and E-spraying produced regular dense films, and E-spinning prepared fiber mat films (Figure 1c-1). Figure S1 shows the macroscopic photographs of the three kinds of films. These films were also characterized by SEM, and the cross-sectional SEM images are shown in Figure 1. Figure 1a-1,b-1,c-2 shows that all three methods yield uniform films, with thickness varying from 200 to 600 μm. The images also indicate the density sequence of the films is 3D-printing > E-spraying > E-spinning (detailed density data can be found in Figure S2). SEM images with higher magnification (Figure 1a-2,b-2,c-3) show that dispersion of Al NPs was the best in the E-spun case and the worst for the 3D-printed case. Al NPs formed aggregates (bright areas, micron) in the 3D-printed case, as shown in Figure 1a-3. While in the E-sprayed sample (Figure 1b-3,b-4), Al NPs formed smaller aggregates (submicron) but poorer contact with PVDF. In the E-spun case (Figure 1c-4,c-5), the Al NPs appeared to be well dispersed and encapsulated in submicron PVDF fibers. Compared to the E-sprayed case, E-spun samples show better contact between Al and PVDF, since Al NPs were attached either outside (E-sprayed) or encapsulated inside (E-spun). Considering the reactivity of heterogeneous energetic materials is highly dependent upon the characteristic heat and mass diffusion distances, the burning rates of these films should be significantly different.

Architecture of Al/AP/PVDF Films: 3D-Printing, E-Spraying, and E-Spinning. To incorporate AP into the Al/PVDF fiber mat and thus increase the energy density, a second vertical E-spraying nozzle with AP/nitrocellulose (NC) solution was employed (Figure 2a). The two nozzles were

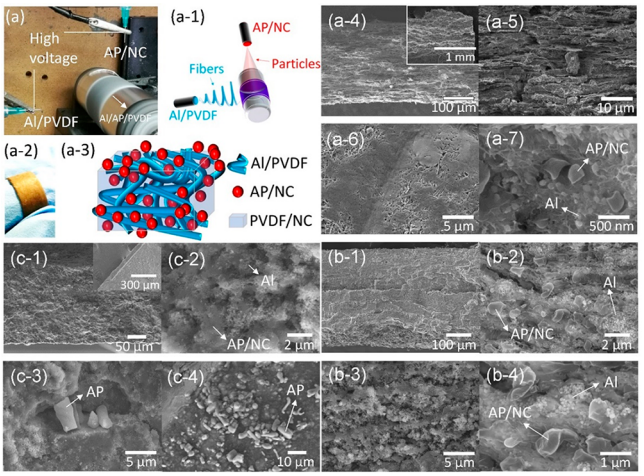

Figure 2. E-spinning/E-spraying dual-nozzle preparation setup (a, a-1) of the Al/PVDF fiber-enforced and AP containing films. The optical photos (a, a-2), the schematic showings (a-1, a-3), and the low and high magnification SEM images (a-4 to a-7). The low and high SEM images of E-sprayed (b-1 to b-4) and 3D-printed (c-1 to c-4) Al/AP/PVDF films with the same formulation as above. Note, that the thicknesses for 3D-printed, E-sprayed, and E-spun films are ~200, ~ 310, and ~310 μm.

well aligned to the center of the substrate at a fixed distance of ~2 cm. The voltages applied on the nozzles and the substrate are +5kv and −5kv, respectively, which successfully produced stable Taylor-cones on both nozzles. As Figure 2a-1 shows, the Al/PVDF nozzle produced fibers, which is the same as the above Figure 1c. While at the same time, the AP/NC nozzle sprayed particles which deposited onto the fibers. Via this approach, a 37% denser film (Figure S2) of Al/AP/PVDF was prepared and is shown in Figure 2a-2. It is important to note, that since the films were wet deposited, the remaining solvent might dissolve minor amounts of PVDF and NC together to form a dense PVDF/NC matrix (Figure 2a-3), which can be seen in the multilayered structures shown in the SEM images in Figure 2a-4,a-5. This effect results in a relatively dense interior of the film. The top-view (Figure 2a-6) of the film also shows a dense surface where fibers were encapsulated by a polymer matrix. A higher-magnification view (Figure 2a-7) shows that the AP/NC particles (~100−300 nm) and Al NPs were well mixed and embedded in the polymer matrix, but

DOI: 10.1021/acsapm.9b00016
ACS Appl. Polym. Mater. 2019, 1, 982−989

since the AP/NC particles are sensitive to the electron beam, they shrink rapidly and peel off from the matrix, as shown in Figure 2a-7.

The low and high-resolution SEM images of Al/AP/PVDF films were also taken for films prepared by E-spraying (Figure 2b-1 to b-4) and 3D-printing (Figure 2c-1 to c-4), for which the formulations are the same as the above. Compared to the E-sprayed and 3D-printed Al/PVDF SEM images shown in Figure 1b,a, the Al/AP/PVDF films in Figures 2b (E-spray) and 2c (3D-print) indicate a more porous structure. The 3-D printed films make the densest films, while the E-spray and fiber composites are mostly comparable, and thus any difference in propagation velocity between the last two systems should be attributable to primarily architecture, while differences between the printed and sprayed for the same general architecture can be attributed to density. For E-sprayed and 3D-printed Al/AP/PVDF cases, the AP/NC particles are ~0.5−1.0 and ~2−8 μm, respectively. All the Al/AP/PVDF films, commercial Al NPs, and PVDF were characterized by XRD, and the results are shown in Figure S3, which confirm that the XRD patterns of the films match the peaks of Al, AP, and PVDF. The 3D-printed Al/AP/PVDF XRD pattern shows much higher and sharper peaks from AP, indicating more complete crystallization of AP in the 3D-printing case, consistent with the SEM results of larger AP particles.

Combustion of Al/PVDF and Al/AP/PVDF Films. The burning rates of all Al/PVDF and Al/AP/PVDF films were measured in argon and captured by a high-speed camera, as seen in Figure 3. The E-spun material clearly has the most

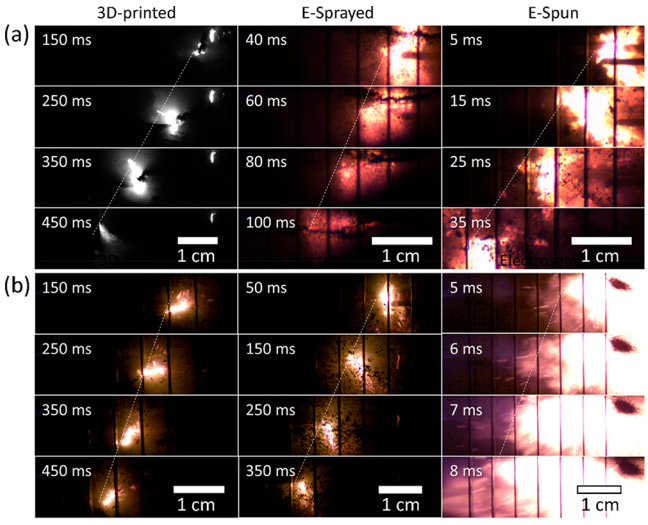

Figure 3. Burning snapshots of Al/PVDF (a) and Al/AP/PVDF (b) films made by 3D-printing, E-spraying, and E-spinning. The labels are the real time after ignition, with the same exposure and framerate.

violent burning with the largest and brightest flame. The E-sprayed has a much dimmer flame, but it is still larger and brighter than the 3-D printed case. The time stamps are the time after ignition, indicating E-spun Al/PVDF and Al/AP/PVDF burn at the highest rates, followed by the E-spray and 3-D printed.

The burning rates of both Al/PVDF (φ = 0.5, 1.0, and 1.5) and Al/AP/PVDF (φ = 1.0) films prepared using the three different methods are shown in Figure 4. In these experiments, Al/PVDF films were combusted in air, argon, and water, while the Al/AP/PVDF films were only combusted in argon. As

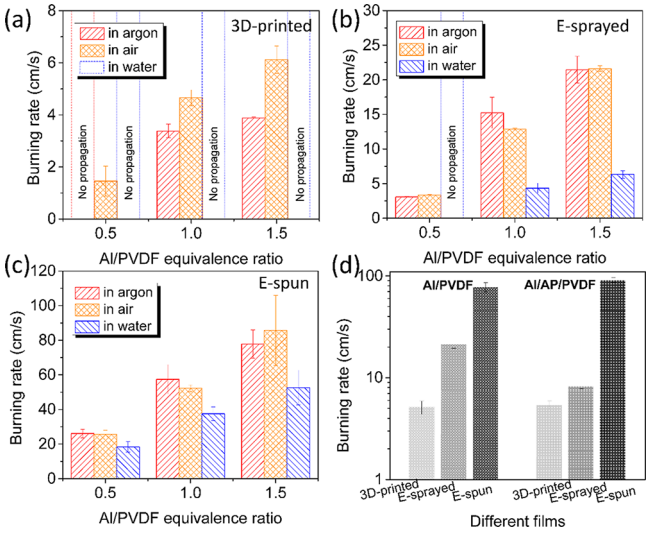

Figure 4. Burning rate of 3D-printed (a), E-sprayed (b), and E-spun (c) Al/PVDF films with different equivalence ratios of 0.5 (fuel lean), 1.0 (stoichiometric), and 1.5 (fuel rich) in argon, air, and water. The comparison (d) of 3D-printed, E-sprayed, and E-spun Al/PVDF and Al/AP/PVDF films (stoichiometric) burning rate in argon.

Figure 4a shows, the burning rates of 3D-printed Al/PVDF films vary from ~1.5 to 6 cm/s, dependent on the equivalence ratio and burning atmosphere. As expected, with the increase of Al content from fuel lean (phi = 0.5, phi means equivalence ratio) to fuel rich (phi = 1.5), the burning rate in air increased 4×. The burning rates in argon are lower than those in air, suggesting incomplete combustion. While the XRD appears to show similar products, it will not pick up the amorphous carbon that is certain to be part of the reaction product. Importantly, the 3D-printed Al/PVDF films do not propagate in water and fuel lean (phi = 0.5) in argon. Al/PVDF made by E-spraying had a linear burning rate ~3 times higher than that of the 3D-printed cases, which range from ~2.5 to ~20 cm/s. All the E-sprayed Al/PVDF propagate in both air and argon with relatively high burning rates, especially when fuel rich (phi = 1.5, ~20 cm/s). Interestingly, the phi = 1.0 and phi = 1.5 cases can also burn in water with a speed of ~5 cm/s (see the Supporting Video). As for E-spun Al/PVDF, the burning rates were in the range of ~20−80 cm/s, which is ~15× and ~4× higher than that of the 3D-printed and E-sprayed, respectively. Even when burning the E-spun Al/PVDF film in water, the burning rates can be as high as ~50 cm/s, for the fuel rich case (phi = 1.5). For the Al/AP/PVDF cases (phi = 1.0), we also measured the burning rates in argon, and the results are summarized in Figure 4d. It also shows the same trend as the Al/PVDF case, where E-spun films burned the fastest, and the 3D-printed films were the slowest. It is worth noting, that the burning rate of the E-spun Al/AP/PVDF film is as high as ~100 cm/s in argon, which is ~17 and ~11× higher than that of the 3D-printed and E-sprayed cases. Differences in the burning rate between the 3-D printed and E-spray may, in large part, be simply attributable to the sprayed material being less dense. However, this cannot be the sole reason, as flame temperature, completeness of reaction, and a significant difference in ignition temperature appear to favor the E-spray material, as will be discussed later. However, the large difference in propagation velocity between E-spray and E-spun, given the minor difference in density, clearly points to the importance of microarchitecture on reaction properties.

DOI: 10.1021/acsapm.9b00016
ACS Appl. Polym. Mater. 2019, 1, 982−989

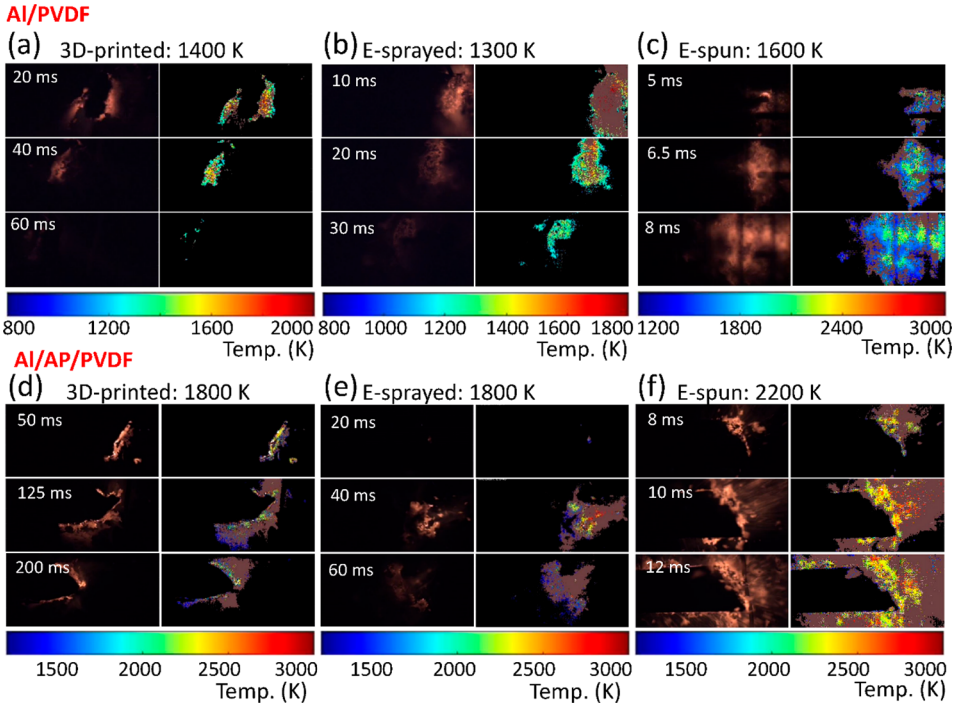

Figure 5. Flame temperatures (median value in all the active points), burning snapshots (labels are the time after triggering), and corresponding temperature maps (with temperature scale bar) of 3D-printed, E-sprayed, and E-spun Al/PVDF (phi = 1.5) and Al/AP/PVDF (phi = 1.0) films. Note, that the length scale for all the snapshots is ~10 mm. Brown areas represent measurements high in error and are intentionally covered.

Flame Temperature of Al/PVDF and Al/AP/PVDF Films. The flame front temperatures of both Al/PVDF (phi = 1.5 was selected for its high burning rate) and Al/AP/PVDF (phi = 1.0) films were obtained by color ratio pyrometry.[3] As shown in Figure 5, all the Al/PVDF films have flame temperatures of ~1300−1600 K, while the Al/AP/PVDF films burn ~400−600 K hotter. Notably, in both cases, E-spun cases had the highest flame temperatures, ~ 1600 K for Al/PVDF and ~2200 K for Al/AP/PVDF, which is >200 K and ~400 K higher than that of the corresponding 3D-printed and E-sprayed case. No differences in the flame temperature between the 3-D printed and E-spray confirm that the density issue cannot be the sole reason. However, the increase of the flame temperature from the E-spray to E-spun case, but with the a minor difference in density (Figure S2), further confirms the importance of microarchitecture on reaction properties. The burning products of both Al/PVDF and Al/AP/PVDF in argon were collected and characterized by XRD (Figure S4) and SEM/EDS (Figures S4 and S5). The XRD in Figure S4 only shows AlF_3 (PDF#47-1659) for both Al/PVDF and Al/AP/PVDF, indicating an efficient reaction between Al/PVDF and Al/AP. However, Al/AP/PVDF cases have a lower carbon residue, indicating more carbon oxidation. Importantly, similar to the reactivity order of E-spun > E-sprayed >3D-printed for both Al/PVDF and Al/AP/PVDF cases, the size of produced AlF_3 also follows the same trend. For example, the 3D-printed Al/AP/PVDF produced ~0.5 μm AlF_3 cubes, while E-sprayed and E-spun Al/AP/PVDF formed <100 and <50 nm AlF_3 spheres (Figure S5), which indicates the 3D-printed case might have enhanced Al sintering during combustion due to poor dispersion and mixing between Al and PVDF. The wider and lower AlF_3 peaks for the E-spun case in the XRD results (Figure S4) also indicate much smaller crystal size.

Thermal Decomposition of Al/AP/PVDF Films. The thermal decomposition of Al/AP/PVDF films prepared by the three different methods as well as NC, AP, and PVDF were characterized by TG/DSC/MS at a heating rate of 10 °C/min to 550 °C. Figure 6a,b shows the TG and DSC results, in

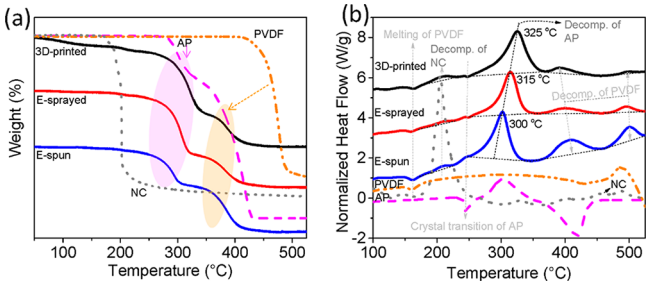

Figure 6. Thermal decomposition results (TG (a); DSC (b)) of AP, NC, and PVDF as well as 3D-printed, E-sprayed, and E-spun Al/AP/PVDF films obtained at a heating rate of 10 °C/min to 550 °C, with an argon flow of 100 mL/min and a heating rate of 10 °C/min.

which NC and PVDF undergo a one-step decomposition at ~200 and ~500 °C, respectively, while AP shows a typical two-step decomposition[18,27−29] which peaks at ~300 and ~420 °C. On the basis of the TG/DSC curves of NC, AP, and PVDF, the Al/AP/PVDF (with 2 wt % NC) thermal decomposition can be divided into three parts, (1) decomposition of NC peaks at ~200 °C, where it releases its maximum thermal energy (Figure 6b) and N_xO_y/CO_2 (confirmed by MS results shown in Figure S6); (2) one-step decomposition of AP peaks at ~300−325 °C, where N_xO_y reaches its maximum (Figure S6); and (3) decomposition of PVDF peaks at ~400 °C (minor decomposition at ~500 °C), where maximum HF was detected (Figure S6). Figure 6a shows that neat AP (pink line)

DOI: 10.1021/acsapm.9b00016
ACS Appl. Polym. Mater. 2019, 1, 982−989

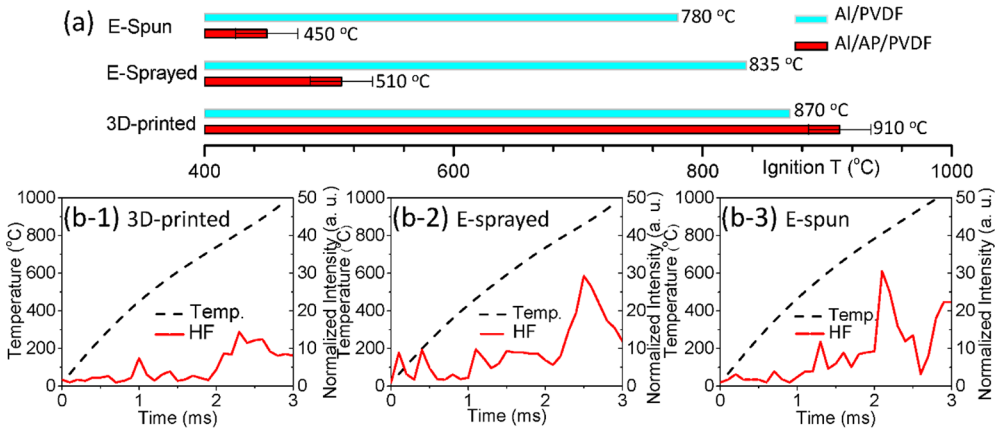

Figure 7. Ignition temperatures (a) of 3D-printed, E-sprayed, and E-spun Al/PVDF and Al/AP/PVDF films. The temperature and HF-release profiles of 3D-printed (b-1), E-sprayed (b-2), and E-spun (b-3) Al/PVDF films obtained from T-Jump TOFMS. Note, that the HF signal was normalized to 133 (fragment from PVDF), see ref 26.

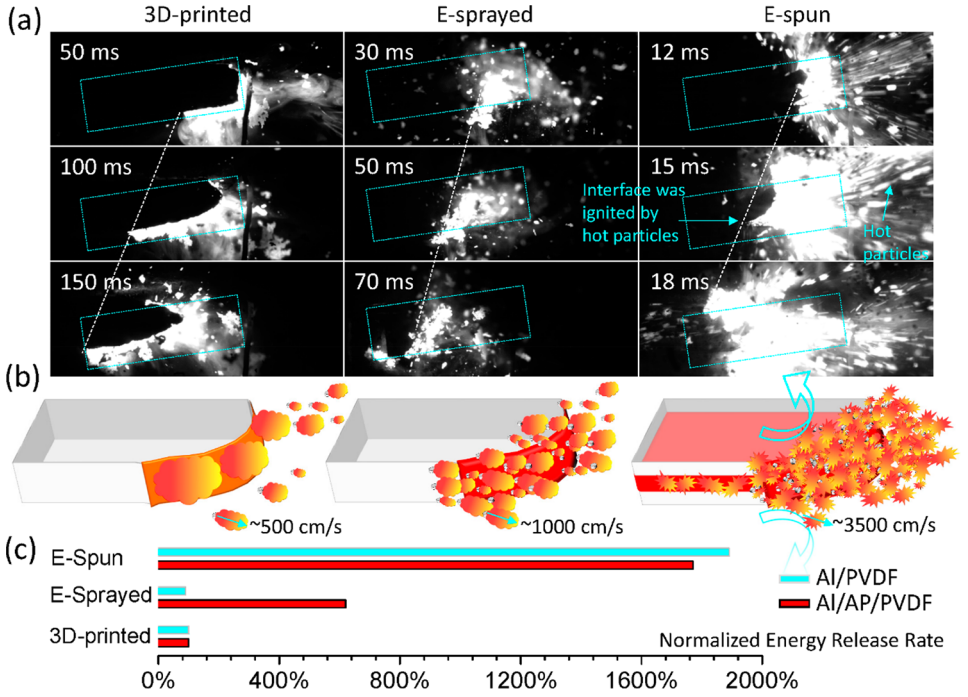

Figure 8. Zoomed-in burning snapshots (a) of 3D-printed, E-sprayed, and E-spun Al/AP/PVDF films (the blue square marks where the film was, whose length is ~10, ~7.5, and ~7 mm, from left to right, respectively). The schematic showing (b) of the burning status of 3D-printed, E-sprayed, and E-spun (from left to right) Al/AP/PVDF films. The relative energy release rate of 3D-printed (set as baseline), E-sprayed, and E-spun Al/PVDF and Al/AP/PVDF films was normalized without the thickness effect.

decomposes at ~400 °C, while the Al/AP/PVDF composite decomposes 100 °C lower (pink shadow). Similarly, neat PVDF (orange line) decomposes at ~475 °C in the composite 100 °C (orange shadow). The DSC curves in Figure 6b and mass spectrum (Supporting Information) results also confirm that the decomposition of AP and PVDF was promoted by ~100 °C. We speculate that the early decomposition of NC is the likely trigger via both energy and reactive oxidizer release. AP decomposition also appears to be matrix dependent, likely due to the difference in the AP particle size.

T-Jump Ignition of Al/PVDF and Al/AP/PVDF Films. Stoichiometric Al/PVDF and Al/AP/PVDF coated on thin platinum wires by the three fabrication methods were used to obtain ignition temperatures at a high heating rate (~4×10^5 K·s^{-1}) in 1 atm argon, as shown in Figure 7a. For Al/PVDF cases, the ignition temperatures vary from ~780 to 870 °C, which is consistent with our previous studies.[26] The E-spun sample has the lowest ignition temperature, and the 3D-printed case has the highest, likely attributable to the increased interfacial contact between Al NPs and PVDF in the E-spun case (as shown in Figure 1). The stoichiometric Al/PVDF-coated wires were also ignited at a high heating rate (~4×10^5 K·s^{-1}) in our T-Jump MS system. The HF release time affects the ignition temperature of Al/PVDF.[26] The time-resolved temperature and HF release profiles, shown in Figure 7b, indicate that the ignition temperature and HF release peak time correspond. With the addition of AP/NC into Al/PVDF, the E-spun and E-sprayed Al/AP/PVDF films show a very significant drop in ignition temperature, as much as 330 °C (ignition snapshots shown in Figure S7). This significant

DOI: 10.1021/acsapm.9b00016
ACS Appl. Polym. Mater. 2019, 1, 982−989

ignition temperature reduction is likely due to the earlier decomposition of AP/NC and PVDF, which release N_xO_y gas and HF 100 °C earlier, as evident in the TG/DSC (Figure 6) and MS (Figure S6) results. However, the 3D-printed Al/AP/PVDF did not see this effect on the ignition temperature, and we can only, at this point, attribute this to the much larger AP crystals (Figure 2c-4).

Effect of Architecture on the Energy Release Rate. In summary, (1) the burning rate of E-spun Al/AP/PVDF is ∼17 and ∼11 times higher than that of the 3D-printed and E-sprayed; (2) the flame temperature of E-spun Al/AP/PVDF is ∼400 °C hotter than that of the other two; (3) the ignition temperatures of E-spun and E-sprayed Al/AP/PVDF are ∼450 and ∼510 °C and are considerably lower than that of the 3D-printed material, ∼910 °C; and (4) the densities of the 3-D printed material are considerably higher than the E-sprayed and E-spun material. Flame temperature is relatively low (∼1800 K) for both 3D-printed and E-sprayed cases, presumably because lower burning rates result in higher radiation loss relative to heat feedback. This leads to the question of which material has the higher energy release rate?

Combining the burning velocity (v), density (ρ), and the cross-sectional area (A), where T is the flame temperature ($\Delta T = T - T_{Ambient}$), we can determine a relative energy release rate

$$R_E = v\rho A\Delta T$$

As Figure 8c shows, despite its higher density, the lower flame speed and temperature actually result in the 3D films having the lowest energy release rate per unit mass, with the fiber-based material far exceeding this. The relative energy release rate of E-spun Al/PVDF compared to the E-sprayed and 3D-printed case is an enhancement of ∼6× and ∼18×, respectively, and the energy release rate of E-spun Al/AP/PVDF is ∼19× higher than that of the E-sprayed and 3D-printed samples. This implies that the lowest density E-spun material offers the highest mass energy release rate by far. The likely explanation for the tremendous enhancement of the energy release rate of the E-spun material is the heat feedback from hot particles that are ejected from the propellent surface at high velocity. This results in a high flame volume, leading to a hotter flame and greater heat feedback to the solid to speed up burning. Our previous results on multilayered materials also found similar results.[4,5] The bright and fast-moving traces (as marked) shown in Figure 8 and the Supporting Video confirm the transport of energy via particles. Keeping in mind, that the particles are likely just being carried by the gas, the particle ejections should occur at the local gas velocity. Particle tracking shows that the 3D-printed case shows relatively slow gas/particles (∼5 m/s), relative to the E-spun material (∼35 m/s). This phenomenon results in the interface layer being ignited easier and propagating much faster than the top and bottom layer for the E-spun case (evidence shown in the Supporting Infomation). This latter point is probably why we have seen in previous studies that multilayer structured films burn faster.[1,2,4,5]

CONCLUSIONS

Al/PVDF and Al/AP/PVDF films with different architectures were prepared by three different techniques, 3D-printing, E-spraying, and E-spinning. AP was also introduced into the Al/PVDF films by the above three different methods to create relatively dense Al/AP/PVDF composite films. The E-spun material showed lower thermal decomposition and ignition temperatures and earlier HF release. Most importantly, however, was that, despite the fact that the E-Spun material had the lowest density, it had the highest burn rate and flame temperature, such that when accounting for these effects, this architecture showed by far the highest energy release rate. The relative energy release rate of E-spun Al/PVDF compared to the E-sprayed and 3-D printed cases is an enhancement of ∼6× and 18×, respectively, and the energy release rate of E-spun Al/AP/PVDF was ∼19× higher than that of E-sprayed and 3D-printed samples. These results point to the critical role that architecture at the nanoscale has on the reaction propagation, energy feedback, and release.

ASSOCIATED CONTENT

Supporting Information

The Supporting Information is available free of charge on the ACS Publications website at DOI: 10.1021/acsapm.9b00016.

Photos of the E-spraying/E-spinning system, typical examples of free-standing films, additional SEM images, film densities, TG-MS data (gas release species) and ignition snapshots of the Al/PVDF and Al/AP/PVDF films, as well as the XRD results and SEM and EDS results of the combustion residues (PDF)

Videos the burning of Al/PVDF and Al/AP/PVDF films in argon (prepared by three methods) (MPG)

Videos of the burning of E-sprayed and E-spun Al/PVDF films in water and zoomed-in burning of Al/AP/PVDF films in argon (prepared by three methods) (AVI)

AUTHOR INFORMATION

Corresponding Author

*E-mail: mrz@engr.ucr.edu.

ORCID

Tao Wu: 0000-0003-3704-275X

Michael R. Zachariah: 0000-0002-4115-3324

Notes

The authors declare no competing financial interest.

ACKNOWLEDGMENTS

This work was supported by DTRA and AFOSR. We acknowledge the support of the Maryland Nanocenter and its NispLab. The NispLab is supported, in part, by the NSF as an MRSEC Shared Experimental Facility.

REFERENCES

(1) Li, X.; Guerieri, P.; Zhou, W.; Huang, C.; Zachariah, M. R. Direct Deposit Laminate Nanocomposites with Enhanced Propellent Properties. *ACS Appl. Mater. Interfaces* **2015**, *7*, 9103−9109.

(2) Wang, H.; DeLisio, J. B.; Holdren, S.; Wu, T.; Yang, Y.; Hu, J.; Zachariah, M. R. Mesoporous Silica Spheres Incorporated Aluminum/Poly (Vinylidene Fluoride) for Enhanced Burning Propellants. *Adv. Eng. Mater.* **2018**, *20*, 1700547.

(3) Yan, S.; Jian, G.; Zachariah, M. R. Electrospun Nanofiber-Based Thermite Textiles and their Reactive Properties. *ACS Appl. Mater. Interfaces* **2012**, *4*, 6432−6435.

(4) Li, X.; Zachariah, M. R. Direct Deposit of Fiber Reinforced Energetic Nanocomposites. *Propellants, Explos., Pyrotech.* **2017**, *42*, 1079−1084.

(5) Wang, H.; Holdren, S.; Zachariah, M. R. Preparation and Combustion of Laminated Iodine Containing Aluminum/Polyvinylidene Fluoride Composites. *Combust. Flame* **2018**, *197*, 120−126.

DOI: 10.1021/acsapm.9b00016
ACS Appl. Polym. Mater. 2019, 1, 982−989

(6) Sullivan, K. T.; Zhu, C.; Duoss, E. B.; Gash, A. E.; Kolesky, D. B.; Kuntz, J. D.; Lewis, J. A.; Spadaccini, C. M. Controlling Material Reactivity Using Architecture. *Adv. Mater.* **2016**, *28*, 1934−1939.
(7) Huang, C.; Jian, G.; DeLisio, J. B.; Wang, H.; Zachariah, M. R. Electrospray Deposition of Energetic Polymer Nanocomposites with High Mass Particle Loadings: A Prelude to 3D Printing of Rocket Motors. *Adv. Eng. Mater.* **2015**, *17*, 95−101.
(8) McCollum, J.; Morey, A. M.; Iacono, S. T. Morphological and Combustion Study of Interface Effects in Aluminum-Poly (Vinylidene Fluoride) Composites. *Mater. Des.* **2017**, *134*, 64−70.
(9) Ke, X.; Guo, S.; Zhang, G.; Zhou, X.; Xiao, L.; Hao, G.; Wang, N.; Jiang, W. Safe Preparation, Energetic Performance and Reaction Mechanism of Corrosion-Resistant Al/PVDF Nanocomposite Films. *J. Mater. Chem. A* **2018**, *6*, 17713−17723.
(10) Slocik, J. M.; McKenzie, R.; Dennis, P. B.; Naik, R. R. Creation of Energetic Biothermite Inks Using Ferritin Liquid Protein. *Nat. Commun.* **2017**, *8*, 15156.
(11) Murray, A. K.; Novotny, W. A.; Fleck, T. J.; Gunduz, I. E.; Son, S. F.; Chiu, G. T. C.; Rhoads, J. F. Selectively-deposited Energetic Materials: A Feasibility Study of the Piezoelectric Inkjet Printing of Nanothermites. *ADDIT MANUF* **2018**, *22*, 69−74.
(12) McClain, M. S.; Gunduz, I. E.; Son, S. F. Additive Manufacturing of Ammonium Perchlorate Composite Propellant with High Solids Loadings. *Proc. Combust. Inst.* **2019**, *37*, 3135−3142.
(13) Ruz-Nuglo, F. D.; Groven, L. J. 3-D Printing and Development of Fluoropolymer Based Reactive Inks. *Adv. Eng. Mater.* **2018**, *20*, 1700390.
(14) Row, S. L.; Groven, L. J. Smart Energetics: Sensitization of the Aluminum-Fluoropolymer Reactive System. *Adv. Eng. Mater.* **2018**, *20*, 1700409.
(15) Padhye, R.; Aquino, A. J. A.; Tunega, D.; Pantoya, M. L. Fluorination of An Alumina Surface: Modeling Aluminum-Fluorine Reaction Mechanisms. *ACS Appl. Mater. Interfaces* **2017**, *9*, 24290−24297.
(16) Valluri, S. K.; Schoenitz, M.; Dreizin, E. Fluorine-containing Oxidizers for Metal Fuels in Energetic Formulations. *DEFENCE TECHNOL* **2019**, *15*, 1−22.
(17) He, W.; Liu, P.; Gong, F.; Tao, B.; Gu, J.; Yang, Z.; Yan, Q. Tuning the Reactivity of Metastable Intermixed Composite n-Al/PTFE by Polydopamine Interfacial Control. *ACS Appl. Mater. Interfaces* **2018**, *10*, 32849−32858.
(18) Wang, H.; Jacob, R. J.; DeLisio, J. B.; Zachariah, M. R. Assembly and Encapsulation of Aluminum NP's within AP/NC Matrix and their Reactive Properties. *Combust. Flame* **2017**, *180*, 175−183.
(19) Wang, H.; Jian, G.; Egan, G. C.; Zachariah, M. R. Assembly and Reactive Properties of Al/Cuo Based Nanothermite Microparticles. *Combust. Flame* **2014**, *161*, 2203−2208.
(20) Yan, S.; Jian, G.; Zachariah, M. R. Electrospun Nanofiber-Based Thermite Textiles and their Reactive Properties. *ACS Appl. Mater. Interfaces* **2012**, *4*, 6432−6435.
(21) Densmore, J. M.; Biss, M. M.; McNesby, K. L.; Homan, B. E. High-speed Digital Color Imaging Pyrometry. *Appl. Opt.* **2011**, *50*, 2659−2665.
(22) Kalman, J.; Hedman, T. On the Origin and Use of The Emissivity Approximations for Alumina Particles. *Propellants, Explos., Pyrotech.* **2016**, *41*, 793−797.
(23) Vision Research, *PHANTOM V21X/V31X/V41X/V61X/V12.1/V71X/Miro310/Miro110 Color & Spectral Response Curve*; http://www.phantomhighspeed.com/Portals/0/Docs/SpectralResponse/spectral-response-V12-X1X-M310-M110.pdf.
(24) Jacob, R. J.; Kline, D. J.; Zachariah, M. R. High Speed 2-Dimensional Temperature Measurements of Nanothermite Composites: Probing Thermal vs. Gas Generation Effects. *J. Appl. Phys.* **2018**, *123*, 115902.
(25) Zhou, L.; Piekiel, N.; Chowdhury, S.; Zachariah, M. R. T-Jump/Time-of-Flight Mass Spectrometry for Time-Resolved Analysis of Energetic Materials. *Rapid Commun. Mass Spectrom.* **2009**, *23*, 194−202.
(26) DeLisio, J. B.; Hu, X.; Wu, T.; Egan, G. C.; Young, G.; Zachariah, M. R. Probing the Reaction Mechanism of Aluminum/Poly (Vinylidene Fluoride) Composites. *J. Phys. Chem. B* **2016**, *120*, 5534−5542.
(27) Mallick, L.; Kumar, S.; Chowdhury, A. Thermal Decomposition of Ammonium Perchlorate-A TGA-FTIR-MS Study: Part I. *Thermochim. Acta* **2015**, *610*, 57−68.
(28) Mallick, L.; Kumar, S.; Chowdhury, A. Thermal Decomposition of Ammonium Perchlorate-A TGA-FTIR-MS Study: Part II. *Thermochim. Acta* **2017**, *653*, 83−96.
(29) Zhu, Y.; Huang, H.; Ren, H.; Jiao, Q. Kinetics of Thermal Decomposition of Ammonium Perchlorate by TG/DSC-MS-FTIR. *J. Energ. Mater.* **2014**, *32*, 16−26.

DOI: 10.1021/acsapm.9b00016
ACS Appl. Polym. Mater. 2019, 1, 982−989